Center Of Mass Motion Of The Cassini Spacecraft Due To Y Axis Turns

by

Marc A. Sengstacke, Ph.D.

California Institute Of Technology
Jet Propulsion Laboratory
301/220G
4800 Oak Grove Dr.
Pasadena, Calif., 91109-8099
(818) 354-0371

August, 1993

Contents

1 Introduction

Attitude maneuvers of a spacecraft generate changes in the spacecraft rotational state [1], [2]. ideally, attitude maneuvers take place without changing the center of mass (CM) velocity, However, in the case of the Cassini spacecraft (which is scheduled for launch to Saturn in October of 1997), thrusters will be used for some attitude maneuvers and they are mounted so as to generate changes in the *CM* velocity. The resultant *CM* velocity changes will significantly alter the spacecraft trajectory. Navigation has to model these changes in order to predict what trajectory the spacecraft will actually follow. For this reason, ROTRAN, a computer simulation package (presented at this conference last year [1]) was developed by this author for JPL navigation. ROTRAN generates the *CM* velocity change resulting from an attitude maneuver using thrusters,

In this report, the velocity change resulting from turns about the spacecraft y axis will be studied. First, a mode] called the ***half angle model*** will be derived which linearly relates the angle between " initial and final CM velocities, θ_v, to the total turn angle magnitude, θ_{ro}. Next, a model will be derived that linearly relates the final *CM* velocity magnitude to the square of the spacecraft rigid body radius of gyration. Finally, comparisons will be made between the above models and results of ROTRAN simulations.

Since the half angle and radius of gyration models are linear, they can be used to compute θ_v and the final velocity magnitude without the cost (albeit greater accuracy) of ROTRAN. A principal goal of this study is to understand the validity and limitations of the above models and when the full power of ROTRAN is needed.

2 General Motion Of The Center Of Mass

In this paper, a general mass is any object of nonzero mass, Fig. (1) shows the case of a general mass at some time t relative to a coordinate system $[I]$ which is assumed to be an inertial frame (a frame in which Newton's laws of motion are valid). Approximating the general mass as a collection of infinitesimally small point masses, each such point mass i will have some well defined position $\vec{r}_i(t)$ and some fixed mass m_i. Thus the total mass is $M = \sum mi$. This leads to the following definition for a special point called the *center of* mass *of the* general mass or more simply, the *center of* mass (also called the CM).

$$\vec{R}_{cm}(t) = \frac{\sum m_i \vec{r}_i(t)}{M} \tag{1}$$

The motion of $\vec{R}_{cm}$ relative to $[I]$ is called *translational motion of the general mass.* This motion is also described by the vector $\vec{V}_{cm}$ below, the *velocity of the* center *of mass.*

$$\vec{V}_{cm}(t) = \frac{d\vec{R}_{cm}(t)}{dt} \tag{2}$$

3 The Cassini Spacecraft Model

A picture of the Cassini spacecraft is shown in Fig. (2). The spacecraft is modelled as a rigid body subject only to forces generated by attitude control thrusters. Thruster firings are controlled by the *Attitude* and *Articulation Control System (AACS)*, the operation of which is also modelled. Each thruster has a position and unit force direction fixed in $[S]$ as shown in Fig. (3) (see also Fig. (2)). The force magnitude of the thrusters are in general different but are taken to be identical for this study. To a first approximation, the thrusters are at the corners of a rectangle parallel to and above the xy plane with sides parallel to the z and y axis. This rectangle is also centered on the z axis. However, as will be seen later, there are deviations from this alignment. Nevertheless, the above approximations will do for the current discussion.

The force magnitude of each thruster is assumed to have a zero rise and fall time and to have a constant force magnitude when on. That is, the force magnitude versus time is a series of rectangular pulsea. Therefore, the force due to thruster k when projected in $[S]$ is either $\vec{0}$ or some constant $\vec{F}_k$. Fig. *(4) shows* the thruster positions and forces in the xz plane when viewed from the $+y$ axis. Note that if thrusters 1 and 4 fire, then the spacecraft will undergo a righthanded (counterclockwise) turn with respect to the y axis. A lefthanded (clockwise) turn can be accomplished using thrusters 2 and 3. Note that this involves using the z facing thrusters to implement y axis turns. However, y turns can also be implemented using x facing thrusters. Specifically, pair 7 and 8 and pair 5 and 6 can be used for right and lefthanded turns respectively. 'J'he use of x and z facing thrusters will be studied in this report.

If the z facing thrusters are used, then they will generate a unit acceleration vector $\hat{\mathbf{a}}_{cm} = \hat{\mathbf{a}}_z$ (Eq. (6)) of the center of mass in the spacecraft -z direction as shown in Fig, (4). If the x facing thrusters are used, then either unit acceleration vector $\hat{\mathbf{a}}_{+x}$ or $\hat{\mathbf{a}}_{-x}$ will apply, depending on the turn direction. $\hat{\mathbf{a}}_{+x}$ and $\hat{\mathbf{a}}_{-x}$ point in the $+x$ and $-x$ direction of the spacecraft, respectively..

An extensive description of the AACS can bc found in references [1] and [2]. However, a brief discussion is in order here. First, consider the case where the frames $[I]$ and [S.] of Fig. (1) have the same origin as a third frame [SC] as shown in Fig. (5). [SC] is called the *command frame* for reasons to be presented shortly. Note that $[S_a]$ defines the actual rotational state of the spacecraft since it is always parallel to the spacecraft frame $[S]$. For this reason, $[S_a]$ will be called the *actual frame*.

In actual operation, the time history of the attitude of [SC] relative to $[I]$ is given to the spacecraft. In addition, the time history of the attitude rate of $[S_c]$ relative to $[I]$ is also sent to the spacecraft. The attitude rate is represented by the angular velocity vector $\vec{\omega}_c$ and is called the *command rate*. The combination of the command frame and command rate is called the command *state*.

The job of the *AACS* is to fire the attitude thrusters so that the frame $[S_a]$ and its angular velocity relative to $[I]$, $\vec{\omega}_a$ (also called the *actual rate*), remain within some specified dead band relative to [SC] and $\vec{\omega}_c$. This is done by a closed loop three axis stabilized feedback system.

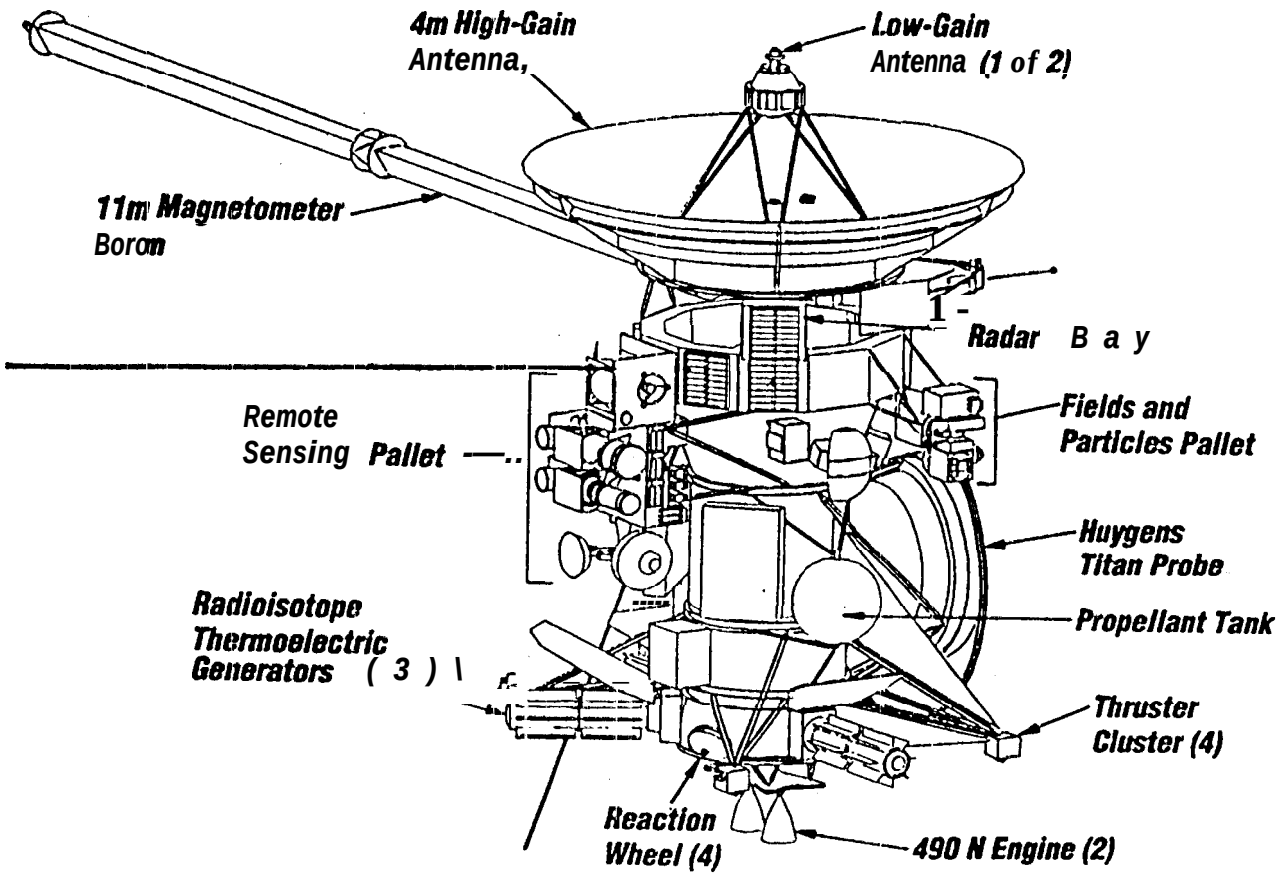

Figure 2: The Cassini spacecraft

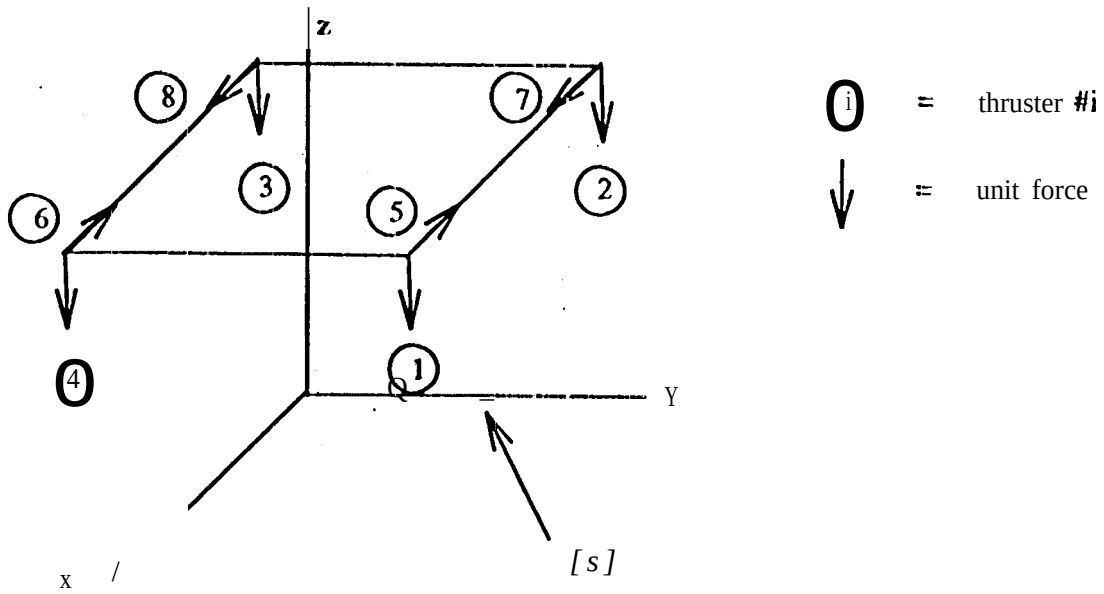

Figure 3: Cassini AACS thruster position and orientation

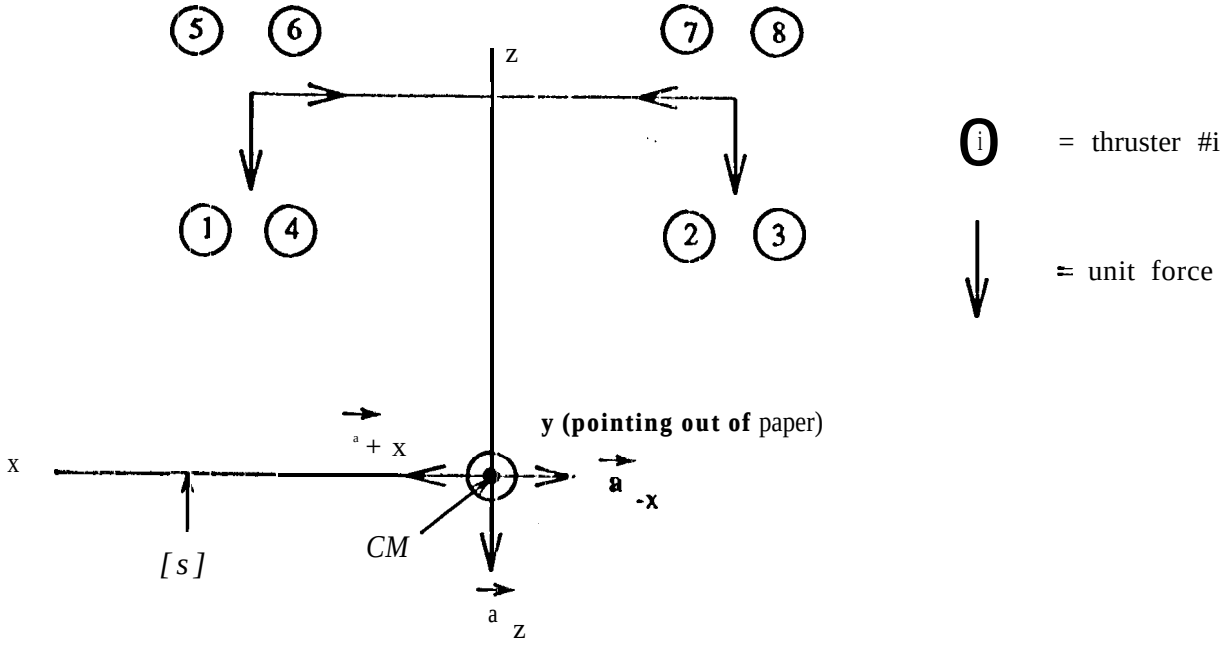

Figure 4: Cassini thruster and unit acceleration geometry viewed from the spacecraft +y axis

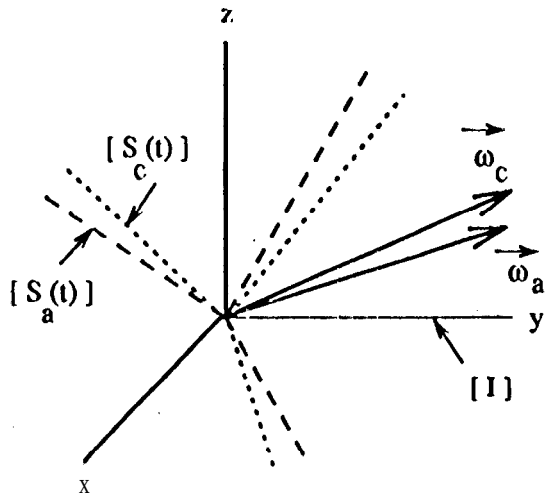

Figure 5: The command, actual and inertial frames

In this study, [Se] is commanded to maintain a common y axis with $[I]$ as shown in Fig. (6). Thus, the command frame and rate are completely defined by θ_r and an angular velocity with a y component only, respectively (in Fig, (6), ω_c is the command rate magnitude). As shown in the figure, WC is set to increase linearly with time from O to ω_m thru time t_a. This time span is called the *acceleration phase*. The magnitude remains constant for a time span t_c, the *constant rate phase*. Finally, the magnitude decreases from ω_m back to O during the *deacceleration phase* over a time span t_d. Defining $t_{ro} = t_a + t_c + t_d$ as the total turn time, the following relates the angle and angular rate (where $O \leq t \leq t_{ro}$).

$$or(t) = \int_0^t \omega_c(t)dt \tag{7}$$

$$\frac{d}{dt}\theta_r = \omega_c \tag{8}$$

Therefore, θ_r exhibits a quadratic, linear and then quadratic behaviour for the three phases. θ_{ro} is the final value of θ_r and is called the *turn angle*.

During any phase of the turn, thruster firings will take place if the command and actual frames are misaligned beyond the dead band. However, thruster activity is expected to be greatest during the acceleration and deacceleration phases and least during the constant rate phase.

4 Dynamics Of A Single Axis Turn

Figs. (7) thru (9) show the translational and rotational state of the spacecraft respectively during the acceleration, constant rate and deacceleration phases of a lefthanded (clockwise) turn about the spacecraft y axis (Fig. (4)). $[I]$ and $[S]$ are respectively the inertial and spacecraft fixed frames of Fig. (l). [S,] is the command frame of Figs. (5) and (6). The frame $[S_a]$ of Fig. (1) is strictly speaking a fourth frame. However, it is assumed that the *AACS* maintains an indistinguishable difference between [S$_c$] and $[S_a]$. Therefore, [S.] is not explicitly shown in this example. $\bar{R}_{cm}$ is the

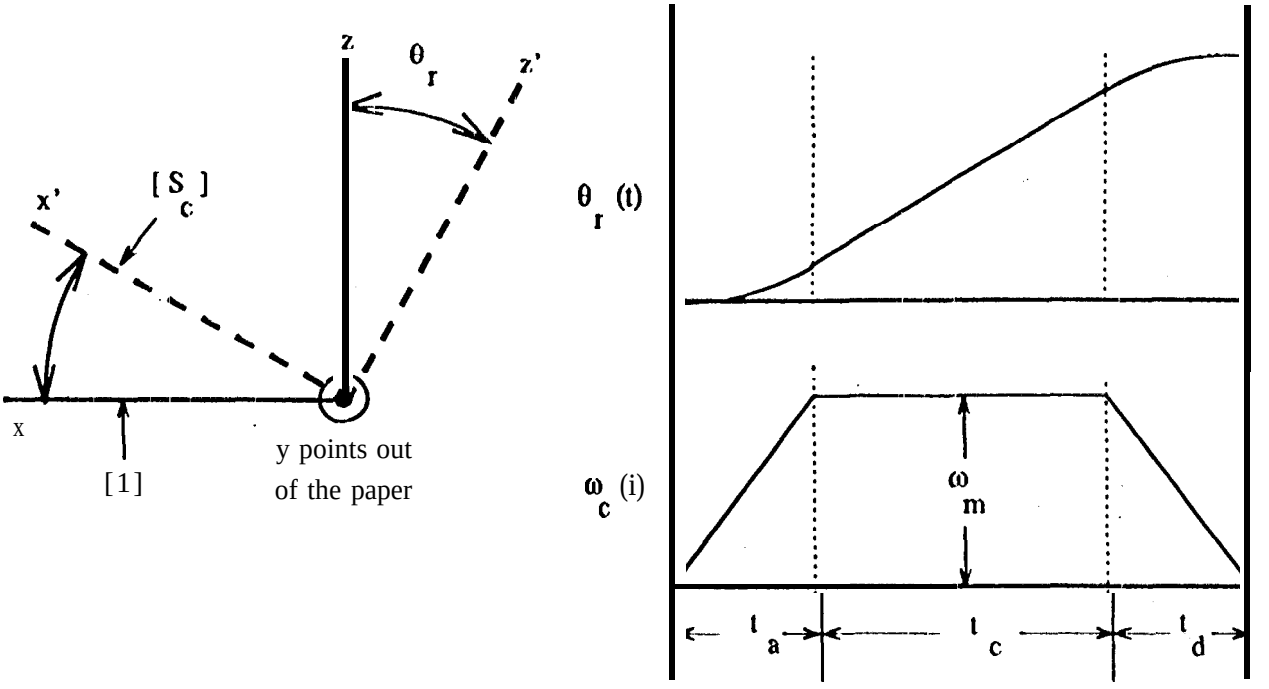

Figure 6: The command frame and rate

center of mass vector. t_a and t_d of Fig. (6) are taken to be equal. In this example, the z facing thrusters of Fig. (4) reused to generate y axis turns. From Fig. (4), this means that the center of mass unit acceleration vector is $\hat{\mathbf{a}}_z$ and is always in the negative z direction of $[S]$. The vector $\hat{\mathbf{a}}_{za}$ is parallel to $\hat{\mathbf{a}}$. However, it has its origin at the origin of $[I]$. At t = O, it is assumed that the *CM* is stationary and that $[S]$ is not rotating relative to $[I]$.

Fig. (7) shows conditions at three successive times t = O, t_1 and t_2 during the acceleration phase. Without loss of generality, the three frames $[I]$, [Se] and $[S]$ are taken to be parallel at t = O. As t increases to t_1, [SC] rotates as shown. Therefore, $[S]$ is instructed to rotate in the same way. In order for this to happen, thrusters 2 and 3 of Fig. (4) must fire. At t = O, this leads to the accelerations $\hat{\mathbf{a}}_z(0)$ and $\hat{\mathbf{a}}_{za}(0)$. At $t = t_1$, $[S]$ will have rotated, hopefully so that $[S_a]$ and [SC] are indistinguishable. This means that, at $t = t_1$, $\hat{\mathbf{a}}_{za}(t_1)$ will also rotate as shown. This covers the rotational change up to t_1. For the translational change, note that the CM will initially move in the $-z$ direction of $[I]$. However, the spacecraft and unit CM acceleration also rotate, Therefore, due to Eq. (6), the CM will shift somewhat as shown. Note that the CM position at t = O is shown in the subfigure for conditions at $t = t_1$ for comparison.

At $t = t_2$, $[S_c]$ has rotated some more. $[S]$ is therefore instructed to keep up, and all vectors change as shown in the figure. The subfigure for $t = t_2$ also shows the CM position at t = O for comparison.

Fig. (8) shows conditions at three successive times t_3, t_4 and t_5 during the constant rate phase. During this phase, [SC] is rotating at a constant rate. Assuming that $[S]$ rotates at the same rate as $[S_c]$ at the start of the phase, then the two frames will rotate together and no thruster firings will be needed. $[S]$ will therefore maintain this constant rate of rotation and $\tilde{\mathbf{V}}_{cm}$ will remain constant due to Eq. (3). The *CM* will thus move in a straight line during this phase.

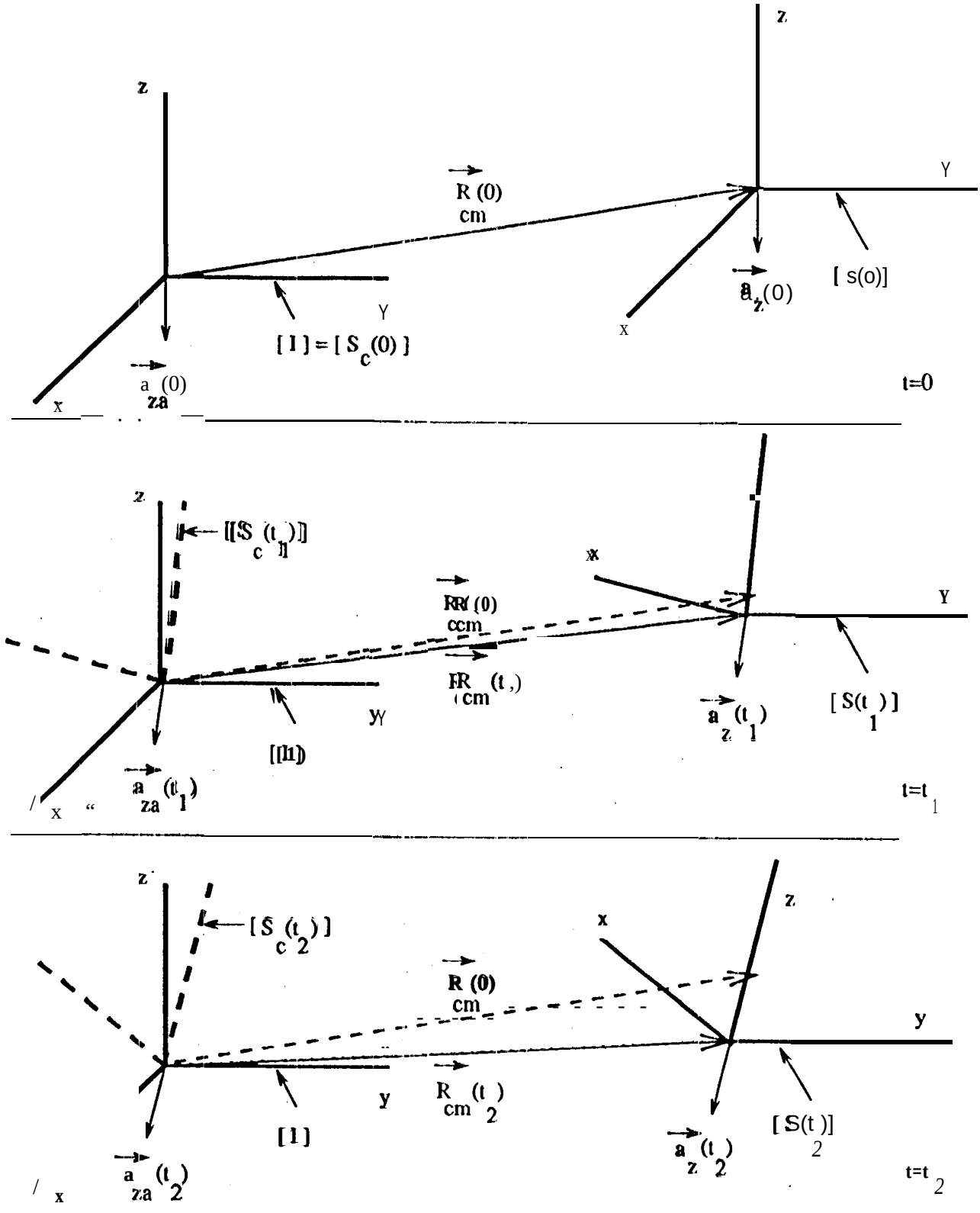

Figure 7: Rotational and translational state - acceleration phase

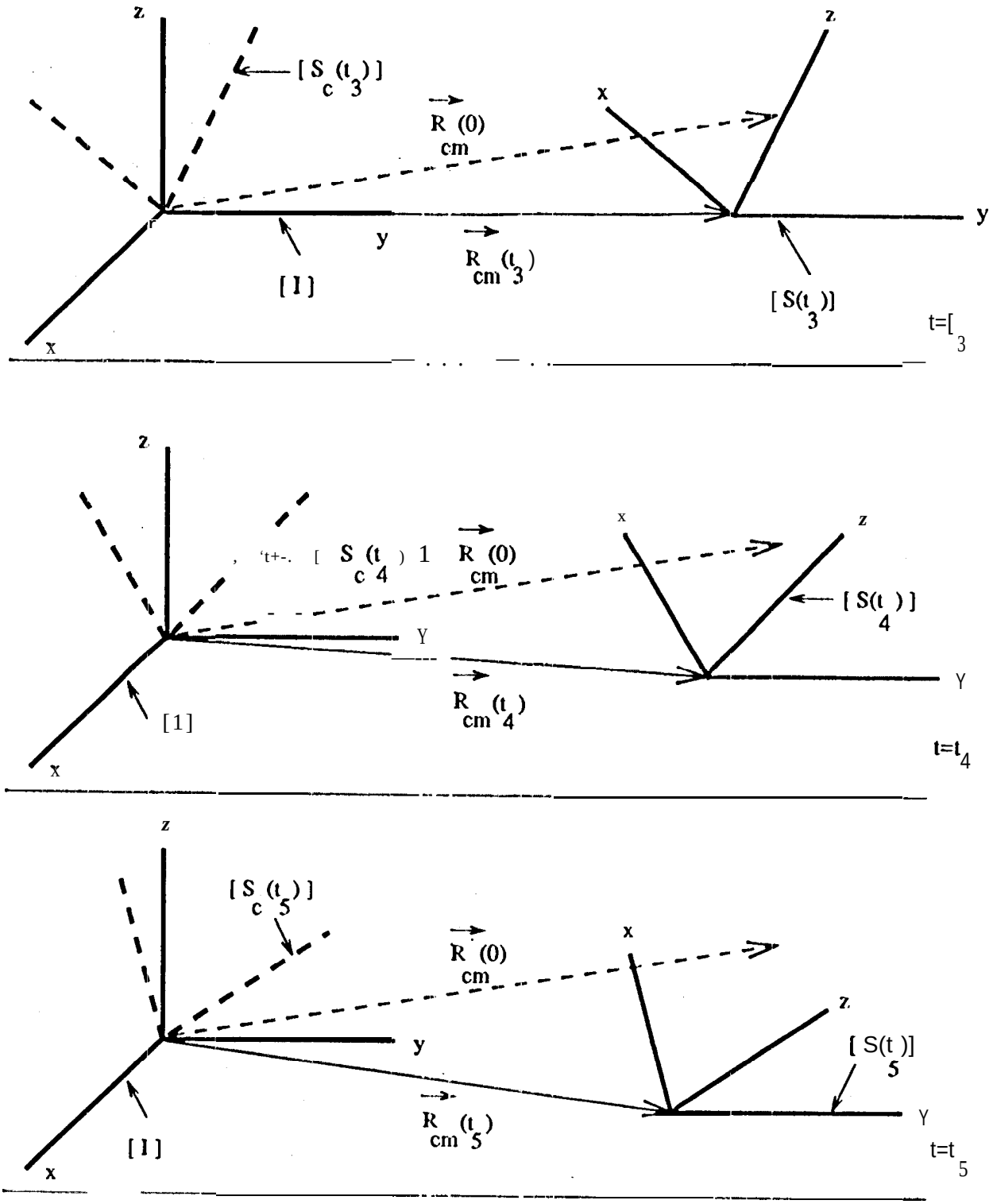

Figure 8: Rotational and translational state - constant rate phase

Finally, Fig. (9) shows conditions at three successive time-s t_6, t_7 and t_8 during the deacceleration phase. During this phase, the rate of rotation of [SC) is slowing down. in order for $[S]$ to do the same, thrusters 1 and 4 of Fig. (4) must fire, yielding the unit acceleration $\hat{\mathbf{a}}_z$ as shown. Recall that the CM moves according to Eq. (6).

5 The Half Angle Formula

5.1 Derivation

The movement of $\hat{\mathbf{a}}_{za}$ in $[I]$ will sufficiently describe the rotational motion in Figs. (7) thru (9) for the purposes of this discussion. Under the above conditions, this vector will remain in the xz plane of $[I]$. Fig, (1 O) shows the variation of $\hat{\mathbf{a}}_{za}$ in this plane as a function of θ_r (which is measured clockwise from the $-z$ axis). θ_a, θ_c and θ_d are the angles between the start and stop values of θ_r respectively in the acceleration, constant rate and deacceleration phases. Note that $\hat{\mathbf{a}}_{za}(\theta_r)$ is shown specifically for a value of θ_r in the deacceleration phase.

From Figs. (6) and (10), Eq. (7) and the condition $t_a = t_d$ in Section (4), one gets the following.

$$\theta_d = \theta_a \tag{9}$$

By definition, the acceleration of Eq. (3) can be written as a magnitude A_{cm} times the unit vector $\hat{\mathbf{a}}_{za}$.

$$\vec{\mathbf{A}}_{cm}(t) = A_{cm}(t)\hat{\mathbf{a}}_{za}(t) \tag{lo}$$

This can be combined with Eq. (3).

$$\vec{\mathbf{V}}_{cm}(t) = \int_0^t A_{cm}(\tau)\hat{\mathbf{a}}_{za}(\tau)d\tau \tag{11}$$

The above can be converted as follows after changing the independent variable from t to θ.

$$\vec{\mathbf{V}}_{cm}(\theta_r) = \int_0^{\theta_r} A_{cm}(\theta)\hat{\mathbf{a}}_{za}(\theta)\frac{d\tau}{d\theta}d\theta \tag{12}$$

It was assumed in Section *(4)* that the spacecraft coasts during the constant rate phase with no thruster activity. '1'bus, $A_{cm}(\theta_r)$ is O for $\theta_a \leq \theta_r \leq \theta_a + \theta_c$. A-ssuming that the thrusters are on continuously during the acceleration and deacceleration phases and assuming conditions outlined in Section (3), one gets from Eqs. (3) and (10) that A_{cm} is constant at A_{cmo} in the acceleration and deacceleration phases. This yields the following result for $\vec{\mathbf{V}}_{cm}$ at the end of the turn when coupled with Eq. (8) and Fig. (,10).

$$\vec{\mathbf{V}}_{cm}(\theta_{ro}) = A_{cmo}\left[\int_0^{\theta_a} \frac{\dot{\epsilon}\,\hat{\mathbf{a}}_{az}(\theta)}{\dot{W}e(e)}\,d\theta + \int_{\theta_a+\theta_c}^{\theta_{ro}} \frac{\hat{\mathbf{a}}_{az}(\theta))}{\omega_c(\theta)}d\theta\right] \tag{13}$$

After an extensive amount of algebra, calculus and geometry, the above can be modified into the next equation with extensive use of the functional dependence of θ_r and ω_c in Fig, (6).

$$\vec{\mathbf{V}}_{cm}(\theta_{ro}) = A_{cmo}\sqrt{\frac{t_a}{2\omega_m}}\left[\int_0^{\theta_a} \frac{(\hat{\mathbf{a}}_{za}(\theta) + \hat{\mathbf{a}}_{za}(\theta_{ro} - \theta))}{\sqrt{\theta}}d\theta\right] \tag{14}$$

It is now convenient to define the following for the sum in the above integrand.

$$A_s(\theta)\hat{\mathbf{a}}_s(\theta) = \hat{\mathbf{a}}_{za}(\theta) + \hat{\mathbf{a}}_{za}(\theta_{ro} - \theta) \tag{15}$$

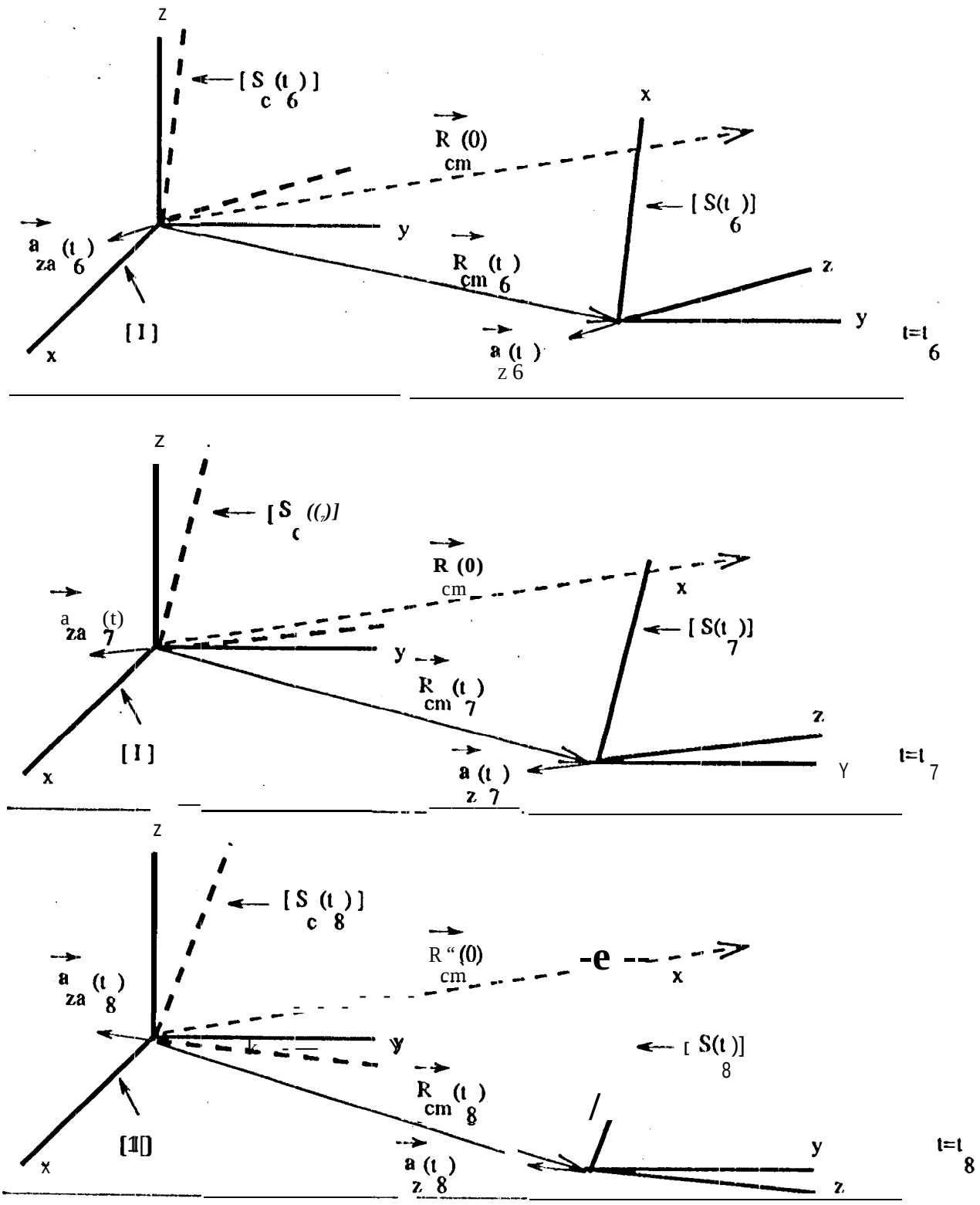

Figure 9: Rotational and translational state - deacceleration phase

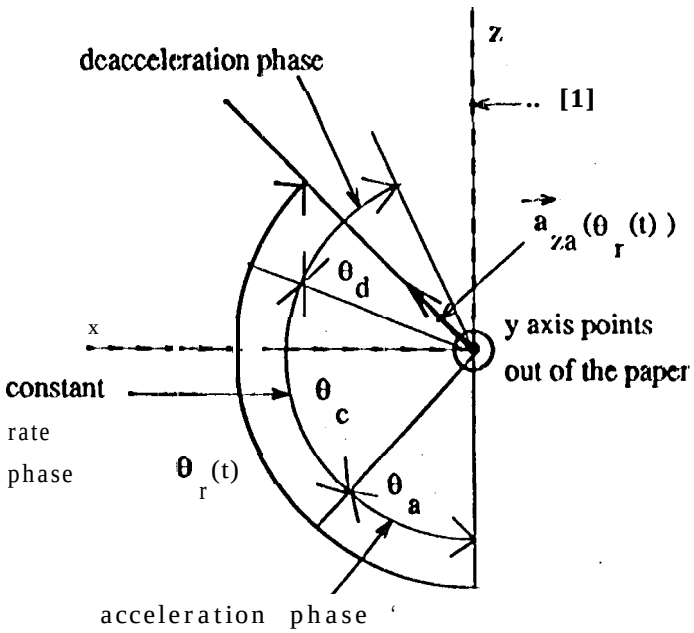

Figure 10: Angular definition of the acceleration, constant rate and deacceleration phases

$A_s(\theta)$ and $\hat{\mathbf{a}}_s(\theta)$ are respectively the magnitude and unit direction of the vector sum on the *RHS* of the above.

The next step is proof that $\hat{\mathbf{a}}_s$ in Eq. (15) is independent of θ. First, note Fig. (1 1). In this figure, the x, y and z axis of [I] are positioned as in Fig. (10). The two unit vectors $\hat{\mathbf{a}}_{za}(\theta)$ and $\hat{\mathbf{a}}_{za}(\theta_{ro}$ -0) on the *RHS of* Eq. (15) are shown. It should be clear that $\hat{\mathbf{a}}_{za}(\theta)$ is rotated by θ clockwise from the - z axis. Similarly, $\hat{\mathbf{a}}_{za}(\theta_{ro} - \theta)$ is rotated by θ counterclockwise from the final angle θ_{ro}. The sum of the two, and therefore $\hat{\mathbf{a}}_s$, will point halfway between $\hat{\mathbf{a}}_{za}(\theta)$ and $\hat{\mathbf{a}}_{za}(\theta_{ro} - \theta)$ forming the angle α as shown. In other words, $\hat{\mathbf{a}}_s$ points at an angle halfway across the rotation angle θ_{ro}, a rotation constant independent of θ in Eq. (15). This allows the following rewrite of Eq. (14).

$$\begin{aligned}\vec{\mathbf{V}}_{cm}(\theta_{ro}) &= \hat{\mathbf{a}}_s A_{cmo}\sqrt{\frac{t_a}{2\omega_m}}\int_0^{\theta_a}\frac{A_s(\theta)}{\sqrt{\theta}}d\theta \\ &= \mathbf{a}_s\, V_{cm}\,(e_{ro})\end{aligned} \tag{16}$$

In other words, the final velocity is in a direction halfway across the full rotation angle $0_{,0}$. From Figs. (4), (7) and (1 1), note that the initial velocity $\vec{\mathbf{V}}_{cm}(0)$ is in the -z direction of [z]. θ_v is the angle between the initial and final velocity. This leads to the following.

$$\theta_v = \frac{\theta_{ro}}{2} \tag{17}$$

This is the form of *the half angle formula* for this case where z facing thrusters are used for y axis turns. When the x facing thrusters are used instead for y axis turns, one gets the following formula after a similar derivation (proof is left to the reader).

$$\theta_v = 90^{\circ} - \frac{\theta_{ro}}{2} \tag{18}$$

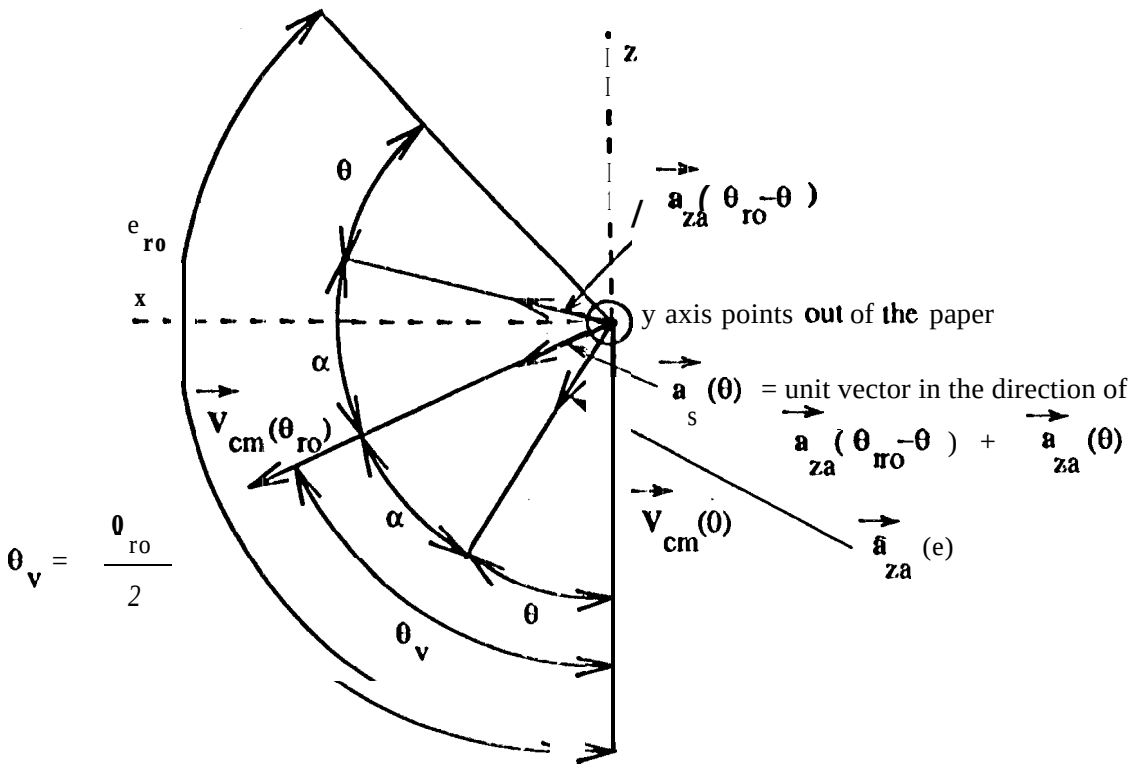

Figure 11: Geometry of the final rotation angle of a turn

This is. still called a ***half angle*** formula since it is linear and the proportionality constant has a magnitude of **1/2.**

5.2 Summary Of Assumptions

The following are assumptions used in the derivation of Eq. (17). A key point in the assumptions is ***symmetry.***

1. The Cassini spacecraft is a rigid body.
2. Forces on the spacecraft are due to attitude control thrusters only.
3. Each thruster has a position and unit force direction fixed in [*S*] (Fig. **(3)).**
4. **Each thruster has the same force** magnitude with a zero rise and fall time. Therefore, the force profile versus time is a series of rectangular pulses.
5. The thrusters are symmetrically located at the corners of a rectangle parallel to and above the xy plane of [*S*] with sides parallel to the x and y axis. 'I'he rectangle is centered on the z axis (Fig. **(3)**).
6. The time of the acceleration and deacceleration phases are equal ($t_a = t_d$ in Fig. (6)).
7. Thrusters fire continuously throughout the acceleration and deacceleration phase but not at all during the constant rate phase.
8. The frames [SC] and [S.] (Figs. (1) and **(5))** are identical.

Note that items (5) thru (8) heavily involve symmetry. These will be referred to in results covered in Section **(8) .**

6 The Relationship Between $\Delta\vec{V}_{cm}$ And The Radius Of Gyrat ion

H_{yy} is the moment of inertia about the spacecraft y axis and M is the spacecraft mass [3]. 'l'his leads to the definition of the radius ***of gyration about the spacecraft y axis***, r_o.

$$r_o = \left(\frac{H_{yy}}{M}\right)^{1/2} \tag{19}$$

Using scalar formulas and several simplifying approximations, a simple relationship between

$$\Delta V_{ro} \equiv \left|\vec{V}_{cm}(\theta_{ro})\right| \tag{20}$$

and r_o can be derived. 'l'he derivation begins with the following for the force on the spacecraft ($\Delta t = 2t_a$ since, by assumption, no forces act during the constant rate phase).

$$F \approx M\frac{\Delta V_{ro}}{\Delta t} \tag{21}$$

The torque eon the spacecraft can be approximated by the following (where r is an effective thruster moment arm and $\Delta\omega = \omega_m$ in Fig. (6)).

$$\begin{aligned} N &\approx H_{yy}\frac{\Delta\omega}{\Delta t} \\ &\approx rF \end{aligned} \tag{22}$$

All the above can be combined to yield a simple expression for AV.

$$\begin{aligned} \Delta V_{ro} &\approx \frac{H_{yy}\Delta\omega}{rM} \\ &\approx \frac{r_o^2}{r}\Delta\omega \end{aligned} \tag{23}$$

The important point from the above is that A V_{ro} is proportional to the square of the radius of gyration for fixed Aw and r. Of course, the above uses a number of simplifications. Nevertheless, the validity of the above will be investigated using two cases where the ratio Aw/r is approximately constant and where r_o is different.

7 Description Of Studied Cases

This study is divided into six cases. Parameters that are constant for all cases are listed in Table(1). Given a specific case, a set of command states are selected. Each command state results in a different turn angle. Given all the above, the command state is fully defined by Fig. (6) where $t_a = t_d$.

Recall that θ_{ro} is the turn angle and is the area under the curve for ω_c in Fig. (6). For a given case and for large turn angles, θ_{ro} is varied by varying t_c from onc command state to the next, maintaining t_a and ω_m at a constant value. This will work for values of θ_{ro} greater than the area under the ω_c curve corresponding to $t_c = O$. The value of θ_{ro} in this case is $\theta_{rc} = \omega_m t_a$. Values of $\theta_{ro} < \theta_{rc}$, are acheived by first setting $t_c = O$ and using the same slope for WC in the acceleration and deacceleration phases as used when $\theta_{ro} \geq \theta_{rc}$. Define ω_a as the value of ω_c at the end of the acceleration phase. The different turn angles for $\theta_{ro} < \theta_{rc}$ are acheived by varying ω_a and t_a within the above slope constraint.

For a given case, ω_m is undefined for $\theta_{ro} < \theta_{rc}$. Nevertheless ω_m is now defined as the peak rate for those turns where $\theta_{ro} \geq \theta_{rc}$ (in this study, all cases have some $\theta_{ro} \geq \theta_{rc}$ so this definition poses no problem). Since this peak rate by construction is the same for all such θ_{ro}, ω_m by the above definition is a case parameter. Note that $\omega_a = \omega_m$ for $\theta_{ro} \geq \theta_{rc}$ and $\omega_a < \omega_m$ otherwise. By the same token, for a given case, the value of t_a is constant by construction for $\theta_{ro} \geq \theta_{rc}$. 'I'his value of t_a is another case parameter and is defined as t_{am}. Given all the above, the next step is to set t_{am}. *However,* a quick review of rotational dynamics is now in order.

The rotational state of a rigid body is completely defined by the Euler equations [3]. In the following, $\vec{\mathbf{N}}$ is the total torque relative to the CM, $\vec{\omega}$ is the angular velocity of a body fixed frame relative to an inertial frame and $\overline{\overline{\mathbf{H}}}$ is the inertia tensor. All vectors and tensors are projected in a body fixed frame $[S]$.

$$\vec{\mathbf{N}} = \vec{\omega} \times \overline{\overline{\mathbf{H}}}\vec{\omega} + \overline{\overline{\mathbf{H}}}\frac{d}{dt}\vec{\omega} \tag{24}$$

Neglecting the first term above and assuming a diagonal inertia tensor, we get (where $i \in (x, y, z)$),

$$\frac{d}{dt}\omega_i = \frac{N_i}{H_i} \tag{25}$$

Parameter	Units	Value		
Control law		Bang/Bang		
Bang/Bang dead band (x,y,z)	radians	$5 * 10^{-4}$	$5 * 10^{-4}$	$5 * 10^{-4}$
Bang/Bang time constant (x,y,z)	seconds	30.0	30.0	30.0
Bang/Bang thruster on time	milliseconds	65		
Sample time	milliseconds	125		
ROTRAN sample time	milliseconds	5		

Thruster Parameters
All thrusters have a z coordinate of +8.0 meters and a force magnitude of 0.6*N*

Thruster number	XY C Coordinates in [S] (meters)		Unit Force in [S]
1	1.26	1.58	$-z$
2	--1.25	1.58	$-z$
3	--1.26	-1.58	$-z$
4	1.25	-1.58	-.?
5	1.26	1.58	$-x$
6	1.25	-1.58	$-x$
7	--1.25	1.58	$+x$
8	--1.26	-1.58	$+x$

Table 1: Parameters constant for all cases

Parameter	Units	Value
Spacecraft mass	Kg	5222.2
Center of mass	meters	-0.03 -0.03 1.38
Inertia tensor	$Kg - M^2$	7625.0 8020.6 3394.8
(xx, YY, zz, xY, xz, yz)		-85.2 137.4 -61.2

Table 2: Beginning Of Mission (BOM) mass properties

Of particular interest in the above equation is the case where $i = y$. For the y axis turns investigated here, one set of thrusters is used in the acceleration phase, another during deacceleration. N_{ya} is the magnitude of the y torque component generated by the acceleration phase thrusters while N_{yd} is correspondingly for the deacceleration phase. Note that N_{ya} is not necessarily equal to N_{yd}.

This study exclusively uses a bang/bang control law [2]. This means that a thruster may or may not fire in a sample period. If it does fire, it is on only for some Δt beginning at the start of the sample period and off for the rest. For a 50% duty cycle, this Δt is half the sample period (However, note in 'I'able (1) that the fraction of the sample period during which thrusters are on is 65/125, a little over 1/2. 'l'his is due to the fact that the thruster on time has to be a multiple of the ROTRAN sample time.). Given a case and therefore an ω_m, the time needed for the acceleration phase thrusters to increase the rate to ω_m from O or for the deacceleration thrusters to decrease the rate to O from ω_m is (using Eq. (25), assuming a 50% duty cycle and where N_y is respectively N_{ya} or N_{yd}),

$$t_{50} = 2\omega_m H_y / N_y \qquad (26)$$

t_{am} is defined to be the larger of the two times above for the two thruster sets. Or equivalently, t_{am} is set baaed on the smaller of N_{ya} and N_{yd}. This way, the thruster set with the smaller torque value will be able to keep up with the command rate in Fig. (6). Note that several assumptions are used to derive the formula used to set t_{am}. However, these assumptions do not matter as long as the chosen value leads to a command state that can be followed by the acceleration and deacceleration thrusters.

In this study, the use of X and Z facing thrusters for y axis turns will be investigated, This study will also use mass properties for expected beginning of mission (BOM) and end of mission (EOM) conditions (Tables (2) and (3) [4]). Finally, two values of ω_m are used, $0.25 deg/sec$ (normal rate) and $0.75 deg/sec$ (sprint rate).

Each case is identified by three character strings. The first string is either X or Z for the thruster set. The second string is either BOM or EOM to identify the mass property. The last string is either normal or sprint to identify the value of ω_m. The cases used for x facing thrusters are (X, BOM, sprint), (X, BOM, normal) and (X, EOM, normal). The cases for z facing thrusters are (Z, BOM, sprint), (Z, BOM, normal) and (Z, EOM, normal). Tables (4) thru (9) contain parameters for each case,

8 Simulation Results

Values of θ_v and ΔV_{ro} versus θ_{ro} for all cases are shown in Tables (10) thru (15). Corresponding plots are shown in Figs. (12) thru (17).

Parameter	Units	Value
Spacecraft mass	Kg	2019.2
Center of mass	meters	0.15 0 0 3 1.16
Inertia tensor (xx, YY, zz, xY, xz, yz)	$Kg - M^2$	5636.5 4727.0 2909.5 -80.5 -34.6 66.6

Table 3: End Of Mission. (EOM) mass properties

Parameter	Units	Value
ω_m	deg/sec	-0.75
N_{ya}	N - M	1.944
N_{yd}	$N - M$	1.944
t_{am}	seconds	108.01

Command State Parameters

θ_{ro} (degs)	t_a (sees)	t_c (secs)	ω_a (degs/sec)
10°	37.95	0	0.2635
20°	53.67	0	0.3726
30°	65.73	0	0.4564
60°	92.96	0	0.6454
90°	108.01	11.99	0.75
120°	108.01	51.99	0.75
150°	108.01	91.99	0.75
180°	108.01	131.99	0.75

Table 4: Parameters for case (X, BOM, sprint)

Parameter	Units	Value
ω_m	deg/sec	0.25
N_{ya}	$N-M$	1.944
N_{yd}	$N-M$	1.944
t_{am}	seconds	36

Command State Parameters

In all cases, $t_a = t_{am}$ *and* $\omega_a = \omega_m$

θ_{ro} ((degs)	t_c (secs)
10°	4
20°	44
30°	84
60°	204
90°	324
120°	444
150°	564
180°	684

Table 5: Parameters for case (X, BOM, normal)

Parameter	Units	Value
ω_m	deg/sec	0.25
N_{ya}	$N-M$	0.2208
N_{yd}	$N-M$	0.2208
t_{am}	seconds	18.68

Command State Parameters

In all cases, $t_a = t_{am}$ and $\omega_a = \omega_m$

θ_{ro} (degs)	t_c (secs)
10°	21.32
20°	61.32
30°	101.32
60°	221.32
90°	341.32
120°	461.32
150°	581.32
180°	701.32

Table 6: Parameters for case (X, EOM, normal)

Parameter	Units	Value
ω_m	deg/sec	0.75
N_{ya}	$N-M$	1.1470
N_{yd}	$N-M$	1.542
t_{am}	seconds	142.84

Command State Parameters

θ_{ro} (degs)	t_a (secs)	t_c (secs)	ω_a (deg/sec)
30°	75.59	0	0.3969
60°	106.9	0	0.5613
90°	130.92	0	0.6874
120°	142.84	17.16	0.75
150°	142.84	57.16	0.75
180°	142.84	97.16	0.75

Table 7: **Parameters** for case (Z, BOM, sprint)

Parameter	Units	Value
ω_m	deg/sec	0.25
N_{ya}	$N-M$	1.470
N_{yd}	$N-M$	1.542
t_{am}	seconds	47.6

Command State Parameters
In all cases, $t_a = t_{am}$ and $\omega_a = \omega_m$

θ_{ro} ((degs)	t_c (secs)
30°	72.4
60°	192.4
90°	312.4
120°	432.4
150°	552.4
180°	672.4

'i'able **8:** Parameters for case **(Z, BOM,** normal)

Parameter	Units	Value
ω_m	deg/sec	0.25
N_{ya}	$N-M$	1.686
N_{yd}	$N-M$	1.326
t_{am}	seconds	31.11

Command State Parameters
In all cases, $t_a = t_{am}$ and $\omega_a = \omega_m$

θ_{ro} (degs)	t_c (secs)
30°	88.89
60°	208.89
90°	328.89
120°	448.89
150°	568.89
180°	688.89

Table 9: Parameters for case (Z, **EOM,** normal)

θ_{ro} ((degs)	θ_v ((degs)	ΔV_{ro} (m/sec)
10	86.10	$4.209 * 10^{-4}$
20	80.01	$1.318 * 10^{-3}$
30	75.06	$2.463 * 10^{-3}$
60	60.17	$7.022 * 10^{-3}$
90	45.14	$1.249 * 10^{-2}$
120	30.16	$1.741 * 10^{-2}$
150	15.19	$2.144 * 10^{-2}$
180	0.18	$2.342 * 10^{-2}$

Table 10: Results of case (X, BOM, sprint)

θ_{ro} (degs)	θ_v (degs)	ΔV_{roo} (m/sec)
10	84.07	$4.174 * 10^{-4}$
20	79.99	$1.136 * 10^{-3}$
30	74.82	$1.830 * 10^{-3}$
60	59.99	$3.845 * 10^{-3}$
90	45.03	$5.598 * 10^{-3}$
120	29.97	$6.959 * 10^{-3}$
150	14.98	$7.858 * 10^{-3}$
180	0.05	$8.207 * 10^{-3}$

Table 11: Results of case (X, BOM, normal)

Plots of θ_v versus θ_{ro} for cases (X, BOM, sprint) and (Z, BOM, sprint) are shown in Fig. (12). The solid lines show the theoretical half angle models for the x and z facing thrusters. Simulated data points are represented by circles and are connected by dashed lines. Note that agreement is very good. However, the slight deviation between simulation and theory for the z facing thrusters can be explained. First, note from Table (7) that $N_{ya} < N_{yd}$. Thus, the acceleration thrusters will have to fire during more sample periods than the deacceleration thrusters in order to generate the same Aw during time t_a. 'I'his means that the contribution to $\vec{\mathbf{V}}_{cm}$ is not the same for the two phases. This violates symmetry conditions listed in Items (5) thru (8) in Section (5.2). Using Fig. (1 1), the reader should be" able to see that this results in a θ_v less than the half angle model for larger turn angles. By contrast, note from Tables (4) thru (6) that $N_{ya} = N_{yd}$ for all three cases using x facing thrusters. This leads to better agreement as can be seen in Figs. (12) thru (14).

Fig. (13) s'hews the same type of plot for cases (X, BOM, normal) and (Z, BOM, normal). The deviation between theory and simulation for z facing thrusters is for the same reason as in Fig. (12) (Table (8)).

Finally, Fig. (14) shows results for cases (X, EOM, normal) and (Z, EOM, normal). In this case, the deviation for z facing thrusters leads to an increase of the simulated θ_v relative to the half angle model. This can be explained by noting from Table (9) that $N_{ya} > N_{yd}$. Therefore, the deacceleration thrusters must fire more often than the acceleration thrusters in order to generate the same Aw during time t_a. It is left to the reader to see that this assymetry leads to the deviation

θ_{ro} (degs)	θ_v (degs)	ΔV_{ro} (m/sec)
10	86.98	$5.892 * 10^{-4}$
20	80.15	$1.511 * 10^{-3}$
30	75.44	$2.468 * 10^{-3}$
60	60.38	$5.156 * 10^{-3}$
90	44.88	$7.493 * 10^{-3}$
120	29.88	$9.311 * 10^{-3}$
150	15.17	$1.043 * 10^{-2}$
180	0.12	$1.092 * 10^{-2}$

Table 12: Results of case (X, EOM, normal)

θ_{ro} (degs)	θ_v (degs)	ΔV_{ro} (m/sec)
30	14.78	$1.669 * 10^{-2}$
60	29.55	$2.232 * 10^{-2}$
90	44.24	$2.476 * 10^{-2}$
120	58.90	$2.288 * 10^{-2}$
150	72.90	$1.677 * 10^{-2}$
180	85.89	$9.549 * 10^{-3}$

'I'able 13: Results of case (Z, BOM, sprint)

θ_{ro} (degs)	θ_v (degs)	V_{ro} (m/sec)
30	14.71	$1.049 * 10^{-2}$
60	29.20	$9.513 * 10^{-3}$
90	43.68	$7.931 * 10^{-3}$
120	57.96	$5.807 * 10^{-3}$
150	70.34	$3.261 * 10^{-3}$
180	62.40	$5.601 * 10^{-4}$

Table 14: Results of case (Z, BOM, normal)

θ_{ro} (degs)	θ_v (degs)	ΔV_{ro} (m/sec)
30	16.72	$1.616 * 10^{-2}$
60	33.89	$1.481 * 10^{-2}$
90	51.34	$1.226 * 10^{-2}$
120	70.64	$8.994 * 10^{-3}$
150	95.96	$5.294 * 10^{-3}$
180	160.5	$2.158 * 10^{-3}$

Table 15: Results of case (Z, EOM, normal)

as shown.

The velocity magnitude versus θ_{ro} is shown for all cases in Figs. (15) thru (17). For z facing thrusters, the general trend can be understood with the aid of Fig. (11). For small turn angles, the acceleration andl deacceleration phases vectorally enhance $\vec{V}_{cm}$ to a first approximation. However, ΔV_{ro} is small since the acceleration arrd deacceleration phases are not that long. For large turn angles, there is significant cancellation due to symmetry, leaving only an x component for a 180° turn angle. This suggests that ΔV_{ro} peaks somewhere between $\theta_{ro} = 0^o$ and 180°. This is basically what is seen in Figs. (15) thru (17). For x facing thrusters, it is left to the reader to see that the acceleration and deacceleration thrusters vectorally cancel for small turn angles, For larger turn angles, the two phases generate a vectoral enhancement. Also, the time of the acceleration and deacceleration phases increases with the turn angle. This suggests that the velocity magnitude will start out at O and increase. Again this is basically what occurs in Figs. (15) thru (17).

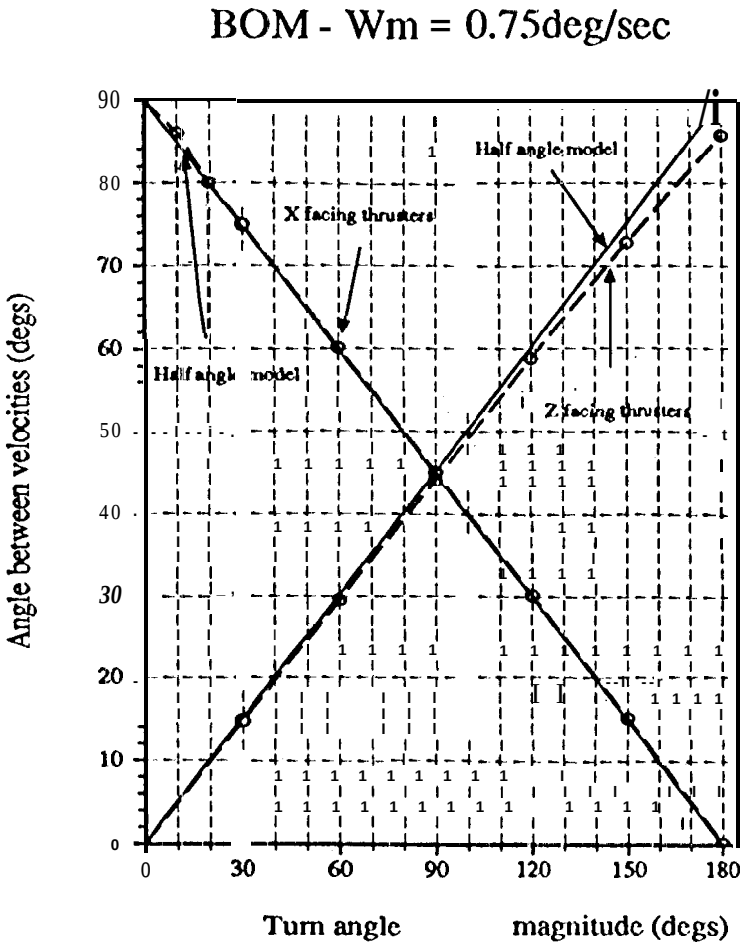

Figure 12: θ_v vs θ_{ro} for cases (X, BOM, sprint) and (Z, BOM, sprint)

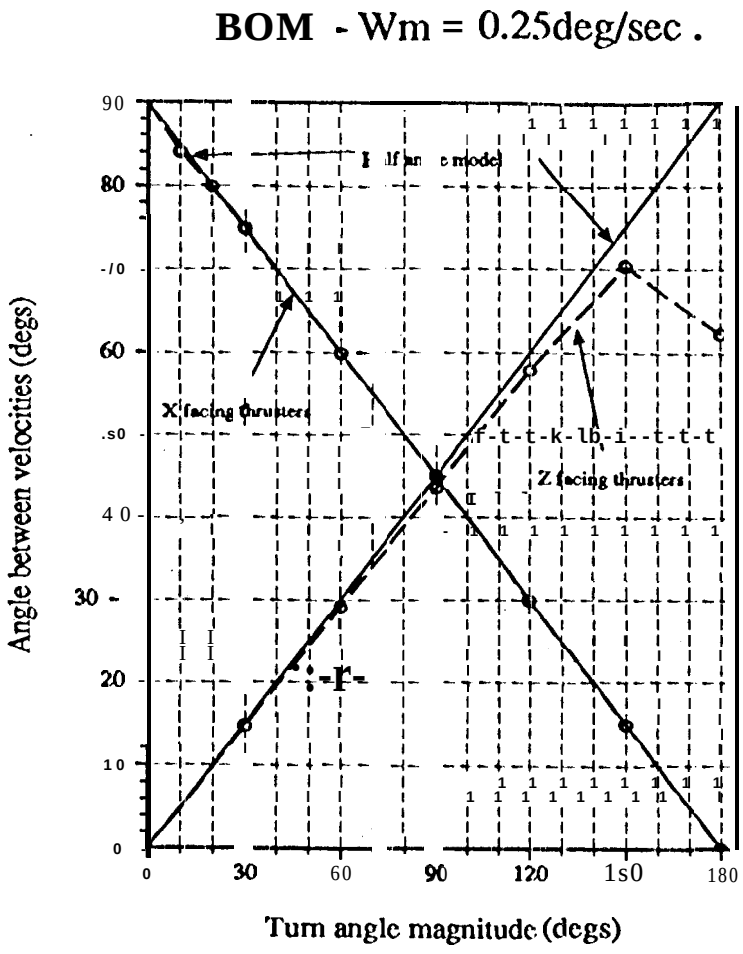

Figure 13: θ_v vs θ_{ro} for cases (X, BOM, normal) and (Z, BOM, normal)

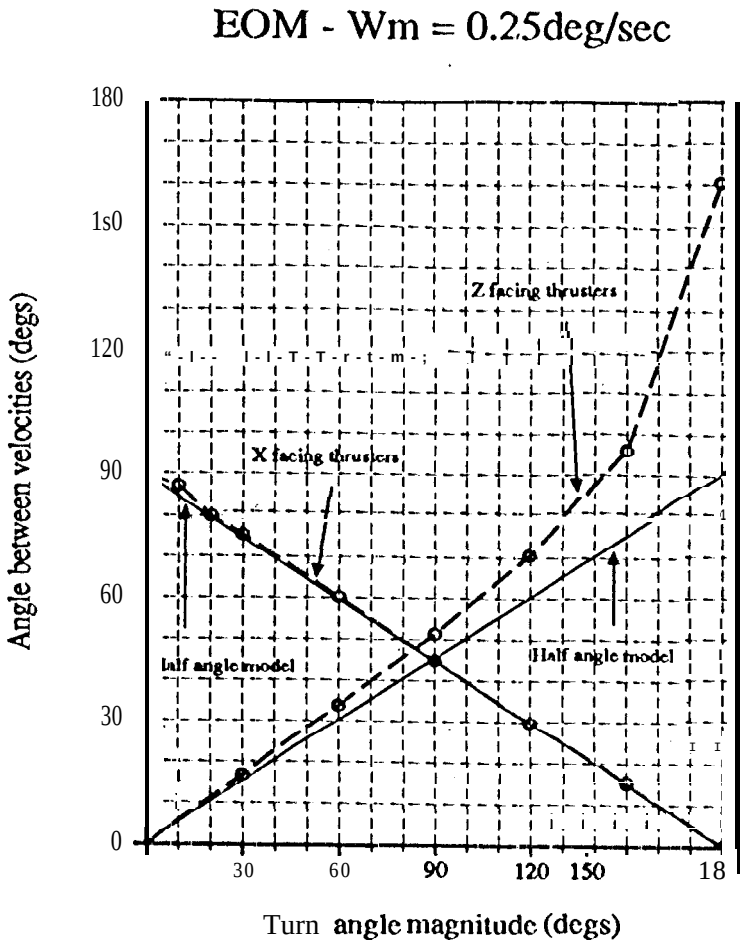

Figure 14: θ_v vs θ_{ro} for cases (X, EOM, normal) and (Z, EOM, normal)

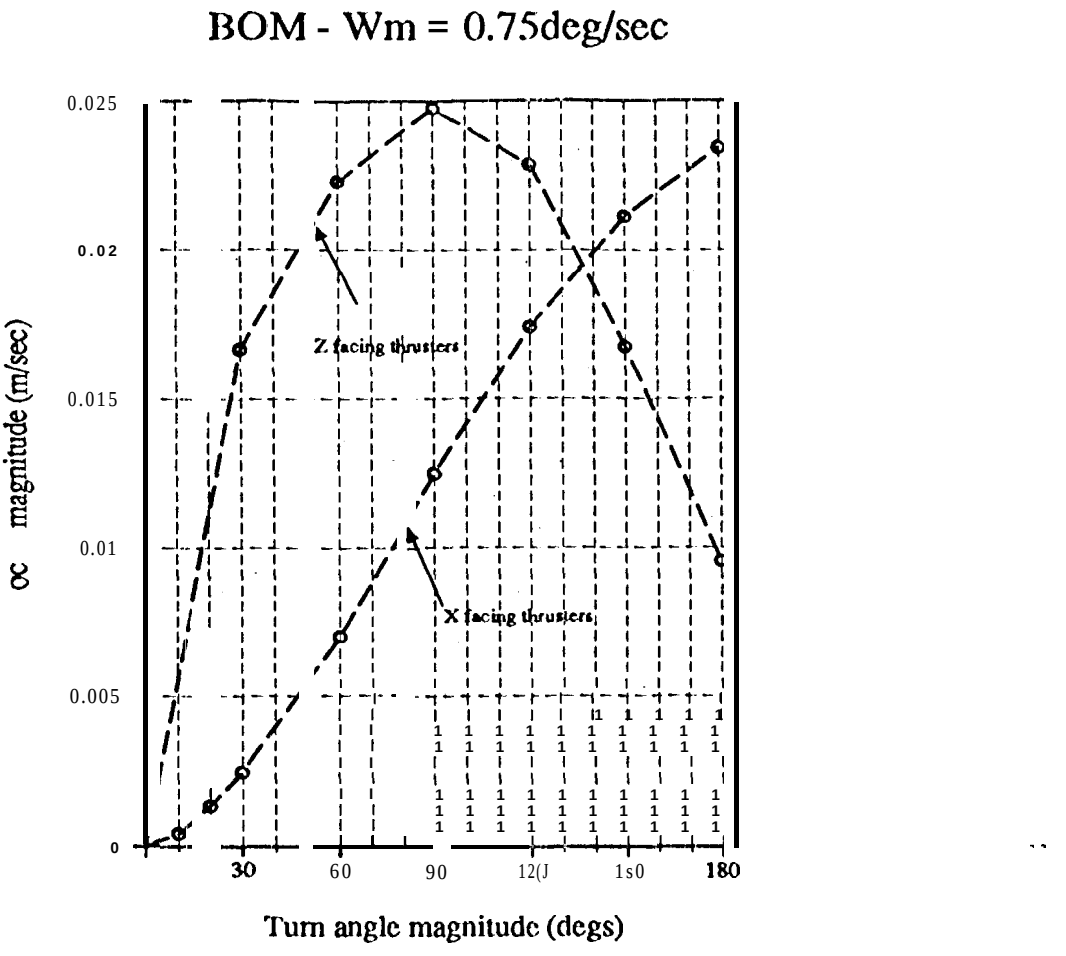

Figure 15: ΔV_{ro} vs θ_{ro} for cases (X, BOM, sprint) and (Z, BOM, sprint)

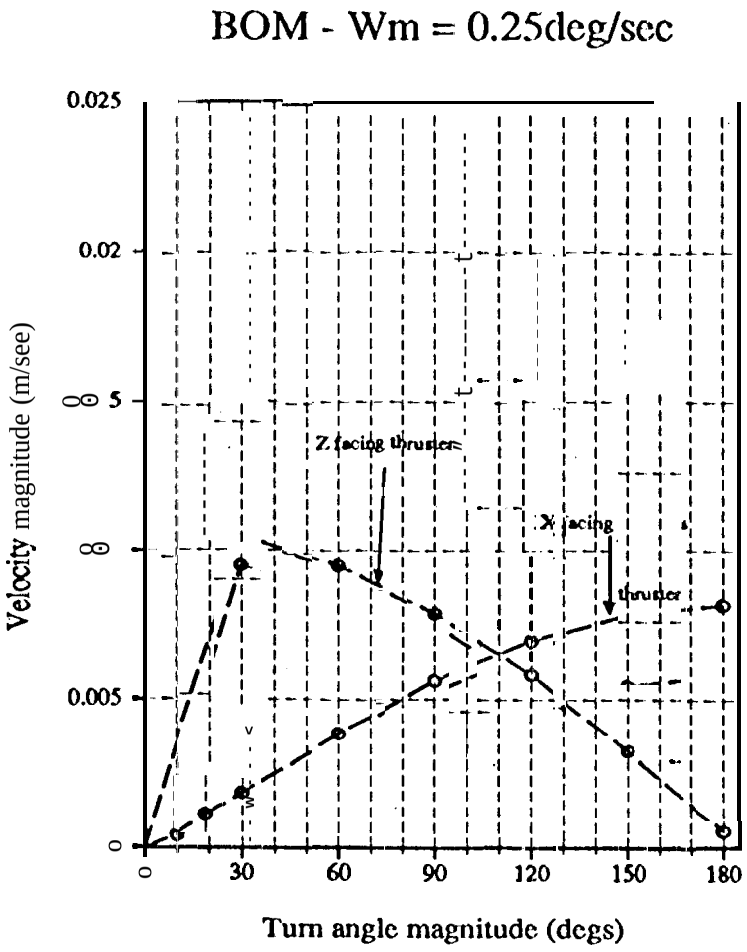

Figure 6: ΔV_{ro} vs θ_{ro} for cases (X, BOM, normal) and (Z, BOM, normal)

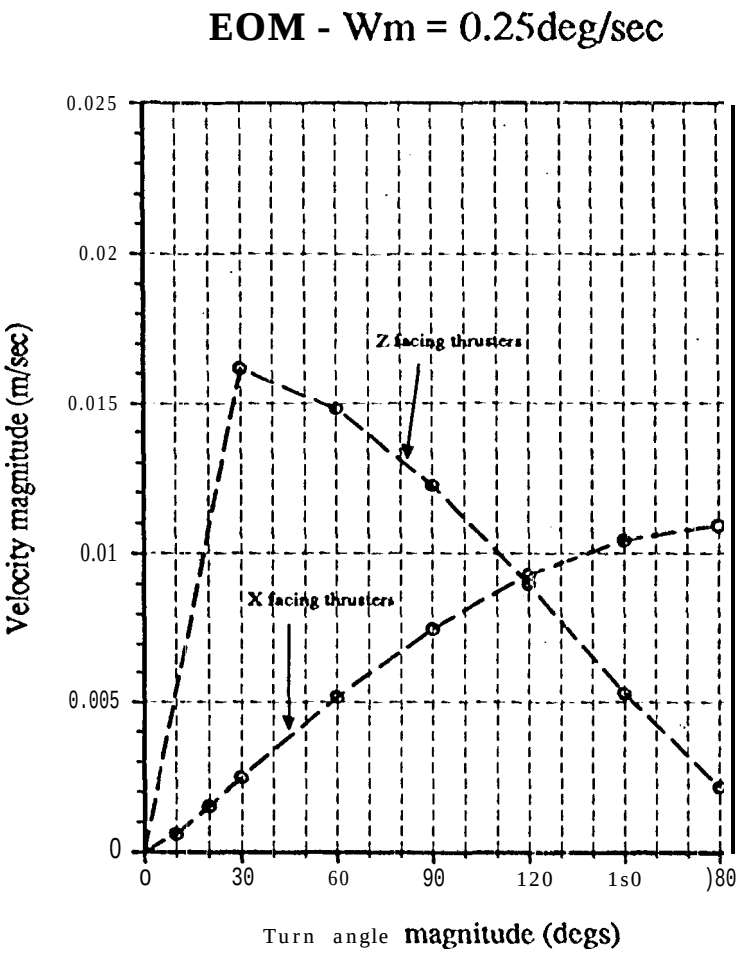

Figure 17: ΔV_{ro} vs θ_{ro} for cases (X, EOM, normal) and (Z, EOM, normal)

This section is concluded with an investigation of Eq. (23). Results arc shown in Tables (16) and (17). TaMe (16) shows results when using x facing thrusters. The column labelled $\Delta V_{ro(EOM)}$ is the velocity magnitude resulting in the case (X, EOM, normal). The column labelled $\Delta V_{ro(BOM)}$ is the velocity magnitude resulting in the case (X, BOM, normal) for the same turn angle. From Tables (5) and (6), all turn angles involve a nonzero value of t_c. Therefore, the peak turn rate is the same for all turn angles, Therefore, the $\Delta\omega$ term of Eq. (23) cancels in the ratio in Table (16). The r term in the equation is an effective moment arm. Note from 'l'able (1) that thruster coordinates in $[S]$ are constant for all cases. However, the CM position depends on which mass property is used, BOM or EOM. However, note from Tables (2) and (3) that the CM offset has a dominant z component which is approximately the same in both cases. Therefore, the r term in Eq. (23) is approximately case independent and will cancel in the ratio in Table (16). This leaves the square of the radius of gyration. This depends only on the mass property. As indicated in Table (16), the ratio of the squares of the radii of gyration is approximately 1.52. This theoretically is the velocity ratio. The ratios in the table are generated by simulation and average out to 1,35. This is considered to be excellent agreement considering the approximations and scalar form of Eq. (23).

Table (17) shows the same results for the z facing thrusters. It is left to the reader to see that all approximations used in Table (16) apply here as well. Excluding the ratio for $\theta_{ro} = 180°$, the average of the simulated ratios is ≈ 1.57 compared to the theoretical value of 1.52 based on Eq. (23). Again, this is considered to be excellent agreement.

$$\left(\frac{r_{o(EOM)}}{r_{o(BOM)}}\right)^2 \approx 1.52$$

θ_{ro} (degs)	$\Delta V_{ro(EOM)}$ (m/sec)	$\Delta V_{ro(BOM)}$ (m/sec)	$\frac{\Delta V_{ro(EOM)}}{\Delta V_{ro(BOM)}}$
10	$5.892 * 10^{-4}$	$4.174 * 10^{-4}$	1.41
20	$1.511 * 10^{-3}$	$1.136 * 10^{-3}$	1.33
30	$2.468 * 10^{-3}$	$1.830 * 10^{-3}$	1.35
60	$5.156 * 10^{-3}$	$3.845 * 10^{-3}$	1.34
90	$7.493 * 10^{-3}$	$5.598 * 10^{-3}$	1.34
120	$9.311 * 10^{-3}$	$6.959 * 10^{-3}$	1.34
150	$1.043 * 10^{-2}$	$7.858 * 10^{-3}$	1.33
180	$1.092 * 10^{-2}$	$8.207 * 10^{-3}$	1.33

$$Average\ of\ \frac{\Delta V_{ro(EOM)}}{\Delta V_{ro(BOM)}} = 1.35$$

'l'able 16: Radius of gyration test using x facing thrusters

$$\left(\frac{r_{o(EOM)}}{r_{o(BOM)}}\right)^2 \approx 1.52$$

θ_{ro} (degs)	$\Delta V_{ro(EOM)}$ (m/sec)	$\Delta V_{ro(BOM)}$ (m/sec)	$\frac{\Delta V_{ro(EOM)}}{\Delta V_{ro(BOM)}}$
30	$1.616 * 10^{-2}$	$1.049 * 10^{-2}$	1.54
60	$1.481 * 10^{-2}$	$9.513 * 10^{-3}$	1.56
90	$1.226 * 10^{-2}$	$7.931 * 10^{-3}$	1.56
120	$8.994 * 10^{-3}$	$5.807 * 10^{-3}$	1.55
150	$5.294 * 10^{-3}$	$3.261 * 10^{-3}$	1.62
180	$2.158 * 10^{-3}$	$5.601 * 10^{-4}$	3.85

$$Average\ of\ \frac{\Delta V_{ro(EOM)}}{\Delta V_{ro(BOM)}} = 1.57\ excluding\ \theta_{ro} = 180°$$

Table 17: Radius of gyration test using z facing thrusters

9 Conclusions

The half angle models of Eqs. (17) and (18) are excellent first order approximate ions under symmetric conditions (Section (5.2)). However, asymmetries due to differences in torque magnitudes of acceleration and deacceleration phase thrusters lead to noticeable and sometimes significant deviations from the half angle formula. The proportionality of the final velocity magnitude to the radius of gyration squared in Eq. (23) is also an excellent first order approximation. The above models enable the first order determination of *CM* velocity characteristics without using the costly albeit greater power of ROTRAN .

References

[1] Sengstacke, Marc A., ***ROTRAN, The JPL*** Navigation ***Cassini Spacecraft*** Simulator, National Council of Black Engineers And Scientist, inc., Technet 1992, compendium of papers.

[2] Sengstacke, Marc A., ***ROTRAN - Theory And Implementation In Software,*** Revision *1,* California Institute of Technology, Jet Propulsion Laboratory, Engineering Memorandum # 314-554, March 19913

[3] Hughes, Peter C., ***Spacecraft Attitude*** Dynamics, John Wiley& Sons, 1986

[4] Lee, Larry W., ***Cassini*** *Project, Project* Mass ***Properties Report, Issue #1,*** Sept. 11, 1992, PD 699-0) 3, California Institute of Technology, Jet Propulsion Laboratory